Down-regulation of tumor suppressor miR-34a contributes to head and neck cancer by up-regulating MET oncogene and modulating tumor immune evasion

Xun Wu
Columbia University Medical Center
Yi-Shing Lisa Cheng
Texas A&M University College of Medicine
Mathew Matthen
Columbia University Medical Center
Angela Yoon
Columbia University Medical Center
Gary K. Schwartz
Columbia University Medical Center
Shashi Bala
University of Massachusetts Medical School
Alison M Taylor
Columbia University Medical Center
Fatemeh Momen-Heravi (f.m.heravi@gmail.com)
Columbia University https://orcid.org/0000-0003-4534-1450

Research

Keywords: Head and neck cancer, miR-34a, aneuploidy, P53, MET

Posted Date: August 25th, 2020

DOI: https://doi.org/10.21203/rs.3.rs-63977/v1

Version of Record: A version of this preprint was published at Journal of Experimental & Clinical Cancer Research on February 17th, 2021. See the published version at https://doi.org/10.1186/s13046-021-

01865-2.

Abstract

Background: MicroRNAs (miRs) have been shown to play an important role in tumorigenesis, including in head and neck squamous cell carcinoma (HNSCC). The miR-34a family is thought to play a role in tumor suppression, but the exact mechanism of action in HNSCC is not well understood. In addition, miR-34a is generally down-regulated HNSCC, but the role of chromosomal changes and mutation status on miR-34a expression remain unknown.

Methods: Differential expression of miR-34a-3p, MET, and genomic alterations were assessed in the Cancer Genome Atlas (TCGA) datasets as well as primary HNSCC and adjacent normal tissue. The biological functions of miR-34a in HNSCC were investigated in samples derived from primary human tumors. The expression of MET was evaluated using immunohistochemistry, and the molecular interaction of miR-34a and MET were demonstrated by RNA pulldown, RNA immunoprecipitation, and rescue experiments. Lastly, mouse xenograft and locked nucleic acid anti-miRs were used to evaluate the clinical relevance of miR-34a in HNSCC tumor growth and modulation of the tumor microenvironment in vivo.

Results: Chromosome arm 1p loss and P53 mutations are both associated with lower levels of miR-34a. In HNSCC, miR-34a acts as a tumor suppressor and physically interacts with and functionally targets the proto-oncogene MET. We found that miR-34a suppresses HNSCC carcinogenesis, at least in part, by downregulating MET, consequently inhibiting HNSCC proliferation. Moreover, ectopic expression of miR-34a reduces HNSCC cell proliferation and tumor burden in vitro and in vivo, represses expression of genes involved in epithelial-mesenchymal transition, and negates the oncogenic effect of MET in mouse tumors. In HNSCC patient samples, higher levels of miR-34a are significantly associated with a higher frequency of Th1 cells, myeloid cells, and regulatory T cells. Consistent with these findings, inhibition of miR-34a in an in vivo model of HNSCC leads to an increased number of immunosuppressive PDL1-expressing tumor-associated macrophages in the tumor microenvironment.

Conclusions: Our results demonstrate that miR-34a directly targets MET and maintains anti-tumor immune activity, and could potentially represent a new therapeutic approach for HNSCC.

Background

MicroRNAs (miR) are evolutionarily highly conserved non-coding RNAs that play roles in fundamental cellular functions by post-translational gene regulation (1). In cancer pathogenesis, miRs exert both anti-tumorigenic and pro-tumorigenic effects by virtue of miR-specific and context-dependent mechanisms. The miR-34 family is considered one of the master regulators of tumor suppression (2). In mammals, the miR-34 family includes three miRs that are encoded by two different genes. miR-34a is encoded by its own transcript, while miR-34b and miR-34c share a common transcript and are dysregulated in some cancers (3). Decreased levels of miR-34a expression have been reported in and linked to the pathogenesis of numerous types of cancer, including ovarian cancer, colorectal cancer, pediatric neuroblastoma,

hepatocellular carcinoma, triple-negative breast cancer, lung adenocarcinomas, bladder cancer, prostate cancer, and osteosarcoma (4–12). The locus harboring the miR-34a transcripts is in a region associated with a genomic fragile site on chromosome 1p. The 1p chromosome arm is frequently deleted in many cancers, including squamous cancers (13).

Recent findings showed that transcription of the miR-34 family is controlled by the tumor suppressor p53; this mechanism links the expression of miR-34 with DNA damage and oncogenic stress (14–16). p53 has multiple binding sites in regions proximal to the *MIR-34A* promoter (17, 18). Other gene regulatory mechanisms, such as CpG methylation of the MIR-34A promoter, have been reported as the main causes of miR-34a down-regulation (14, 19, 20). Mechanistic studies demonstrated that miR-34a itself is a key player in the p53 network, mediating the biological function of p53 by regulating the expression of different genes (21). miR-34a directly suppresses HDM4, a potent negative regulator of p53, forming a positive feedback loop acting on p53 (22). Treatment with a miR-34a inhibitor attenuates p53-mediated apoptosis in response to genotoxic stress, whereas the ectopic expression of miR-34a causes a significant reprogramming of gene expression and induces apoptosis and cell cycle arrest (23). miR-34a has been shown to directly target the 3' UTRs of numerous mRNAs with roles in oncogenesis beyond p53, including Bcl-2, PIK3R2, c-Myc, SIRT1, VAMP2, IKBKE, MYH9, KLRK1, CD11A, SDK4-6, Notch1, TRAFD1, and CCR1 (23–27), which may contribute to its tumor-suppressive function.

In Head and Neck Squamous Cell Carcinoma (HNSCC), miRs can serve as biomarkers for diagnosis and prognosis(28–30). Reduction of miR-34a was detected in HNSCC cell lines and tumor tissues, and was associated with cell proliferation and angiogenesis (31). However, the genetic alterations and molecular network which cause miR-34a downregulation in HNSCC are not well understood. Moreover, the mechanistic role of miR-34a downregulation in the pathogenesis of HNSCC and the tumor microenvironment is not well established.

Our bioinformatic and experimental analyses identified several genes, including the MET proto-oncogene, that are directly regulated by miR-34a. This regulation has implications for the role of miR-34a in modulating tumor repression and the tumor microenvironment. MET is a receptor tyrosine kinase (32), deregulated in many types of human malignancies, including breast cancer, lung cancer, bladder cancer, hepatocellular carcinoma, and melanoma (33, 34). Although abnormal activation of MET in some cancers, such as hepatocellular carcinoma, is known to be correlated with poor prognosis (35), the role of the miR-34a-MET axis in HNSCC has not been investigated. Additionally, the role of miR-34a in the tumor microenvironment in head and neck cancer is also yet to be elucidated. Although miR-34a based therapeutics have been brought to melanoma clinical trials as a first-in-class miR therapy (36, 37), its expression, clinical significance, and molecular mechanisms in HNSCC remain unexplored. In the present study, we determined that miR-34a suppresses HNSCC growth by inducing cell cycle arrest and senescence, and we identified a miR-34a regulatory function in tumor-associated immune cells to elicit anti-tumor immunity.

Materials And Methods

TCGA samples

Our analysis included the TCGA pan-cancer atlas dataset. The following data is available at gdc.cancer.gov/node/977: cancer type, p53 mutation status, chromosome arm aneuploidy status, miR-34a expression, and mRNA gene expression. Estimation of individual immune subtype fractions by xCell in TCGA samples is publicly available at xcell.ucsf.edu (38). The effect of MET expression on survival data was assessed in TCGA data using UALCAN portal (39).

Gene Set Enrichment Analysis (GSEA)

Genes that correlated with miR34 expression with a Bonferroni corrected p-value of < 0.01 were analyzed by the GSEA pre-ranked algorithm (40).

Clinical samples

Clinical samples and plasma were obtained from the tumor bank of Columbia University Irving Medical Center, Biomarker Core of Herbert Irving Comprehensive Cancer Center or University of Massachusetts Medical School Conquering Diseases Biorepository. All samples were collected based on an institutional review board guideline.

LNA-anti-miR-34a synthesis

For LNA-anti-miR-34a, the following 15-mer sequence was syntheized using a phosphorothioate backbone, as described (41): 5´- AgCtaAGacAcTgCC – 3´ (DNA lowercase, LNA uppercase), which targets explicitly miR-34a. The two LNA-controls were synthesized with the following sequences: 5´- TcAtaCTatAtGaCA – 3´ and 5´- TCATACTA – 3´ (DNA lowercase, LNA uppercase). The LNA-control sequence showed no perfect match binding sites in the whole transcriptome based on different databases, and has been validated in different studies and demonstrated no difference compared to untransfected or saline samples in vitro and in vivo (41).

In vitro pull-down assay

miR-34a biotin labeled probe was synthesized by IDT with the probe sequence of 5'Biotin-TGG CAG TGT CTT AGC TGG TTG T as well as the negative control probe with the sequence of 5'Biotin-ACG TGA CAC GTT CGG AGA ATT. RNA samples isolated from CAL27 cells using TRI reagent (Zymo) and treated with DNase I according to the manufacturer's instructions. Biotin-labeled miR-34a pull-down probe or a negative control probes in the final volume of 100 ul and concentration of 1, 0.5, or 0.25 uM were used. 20 ug of RNA was incubated with probe for 1 h at 4 °C. A μMACS separator (Miltney) was used for purification following the manufacturer's protocol. The levels of pulled-down MET were quantified by a real-time RT-PCR assay and normalized to the total input.

Generation of standard curves for absolute quantification of miR-34a-5p and miR-34a-3p

Synthetic cel-miR-39, miR-34a-5p mimic, and miR-34a-3p mimic (Applied Biosystem) were serially diluted to final concentrations of 300 nM, 30 nM, 3 nM, 0.3 nM, 0.03 nM, 3 pM, 0.3 pM, 0.03 pM, 3 fM, and 0.3 fM. miR-34a-5p, miR-34a-3p, and cel-miR-39 serial dilutions were reverse-transcribed and assayed using real-time PCR analysis concurrently with RNA extracted from tumor samples and normal tissue. 2.5 μL of

exogenous cel-miR-39 at a concentration of 200 amol/µl was introduced as an exogenous normalizer before RNA extraction in all samples. Standard curves for miR-34a-5p and has-miR-34a-3p and cel-miR-39 were included on each plate of the miR-TaqMan assays to convert the CT values of each sample into the corresponding number of miR copies. The absolute quantification result of miR-34a-5p and miR-34a-3p was obtained by normalization to cel-miR-39.

Tumor model

All experimental procedures were approved by Institutional Animal Care and Use Committees. Six-week old female nude mice (NU/J) were purchased from Jackson Laboratories. After one week of adaptation, animals were inoculated with FaDu tumor cells (2×10^6 cells in 100 ul volume) subcutaneously on the right flank. Tumor volume was measured continuously from day 4 post implant to following the development of tumors. Five days post implantation of tumor cells, mice were dosed with LNA-anti-miR-34a or LNA-anti-miR-34 (20 mg/kg/day s.c.) for 2 days followed by treatment every 72 h (10 mg/kg s.c).

Immunohistochemistry

Paraffin-embedded human-epithelial tissues, HNSCC tissues, and dysplastic oral squamous cell tissues were immunostained for MET protein using a laboratory established protocol. Briefly, deparaffinization, sequential ethanol treatment and antigen retrieval was performed. The process was followed by blocking and inactivating endogenous peroxidase with 3% H_2O_2, addition of the primary antibody (overnight; 4 °C) and addition of biotin-labeled secondary antibody (Room temperature; 30 min). DAB was used for staining.

Western blot

Western blots were performed using the following established laboratory protocols.Cells were lysed in RIPA buffer and protein was quantified using a Bradford assay (Thermofisher). Proteins were separated using 10% SDS-PAGE electrophoresis and transferred onto polyvinylidene difluoride (PVDF) membranes. The membranes were blocked with 5% nonfat milk and incubated at 4 °C overnight with MET antibodies (1:1000, Abcam). The membranes were then re-incubated with anti-rabbit (1:5000) secondary peroxidase-labeled antibodies at room temperature for 2 h. The blots were visualized with ECL Plus reagent (Bio-Rad).

Exosome isolation

Exosomes were extracted from plasma using an established protocol. Plasma samples were centrifuged at 1,500 g for 10 minutes at 4 °C to remove the cellular debris and then at 10,000 g for 20 minutes to remove the large vesicles. The supernatant was collected and incubated with ExoQuick™ overnight at 4 °C. The mixture was centrifuged twice at 1,500 g for 30 minutes to pellet the exosomes. The pellet was finally resuspended in 200 µl of PBS and used for RNA isolation. For the isolation of exosomes from THP-1 culture medium, supernatant were centrifuged at 700 g for 15 min to deplete cells and then at 12,000 g for 30 min to eliminate residual cellular debris, as described previously. The resulting supernatant was passed through 0.4 µm and 0.22 µm filters and concentrated using the Amicon Ultra-15 Centrifugal Filter

Unit with Ultracel-100 membrane (Millipore, MA). Loading of exosomes with miR-34a-5p mimic or control mimic was performed based on our optimized lab protocol, as described previously.

RNA isolation

RNA from cells, exosomes, and plasma was isolated using a QIAzol Lysis reagent and total RNA was isolated using Direct-zol™ RNA MiniPrep isolation kit. 100 µL of exosome suspension or plasma from plasma of patients with HNSCC or healthy subjects were mixed with 300µL QIAzol lysis buffer, and the mixture was processed according to the standard protocol. Quantity and quality of the RNA were determined by NanoDrop 1000 (260/280 and 260/230 ratios).

Quantitative real-time polymerase chain reaction (qPCR)

qRT-PCR was used to confirm the expression levels of mRNAs and miRs. For mRNA analyses, cDNA was transcribed from 1 µg of total RNA utilizing iScript™ cDNA synthesis kit (Bio-Rad). Real-time quantitative PCR (qPCR) was performed with iTaq Universal SYBR Green Supermix (Bio-Rad). The primer sequences were as follows: Met (forward) 5-GAG GCA GTG CAG CAT GTA GT-3′, Met (reverse) 5′-GAT GAT TCC CTC GGT CAG AA-3′; GAPDH (forward) 5′-TCA GTG GTG GAC CTG ACC TG-3′, GAPDH (reverse) 5′-TGC TGT AGC CAA ATT CGT TG-3′. 18 s mRNA levels were used for normalization. mRNA relative levels were calculated using the ΔΔCt method. The relative expression level of each mRNA was presented by $2^{-\Delta\Delta Ct}$.

microRNA analysis

TaqMan microRNA Assays (Applied Biosystems) was used for detection of miR-34a-3p and miR-34a-5p expression according to manufacturer's protocol. Briefly, reverse transcription (30 min, 16 °C; 30 min, 42 °C; 5 min 85 °C) was performed using a TaqMan stem loop primer, 15 ng RNA, TaqMan primers and miR reverse transcription kit (Applied Biosystems). Quantitative real-time PCR was performed using the TaqMan Universal PCR Master Mix according to the manufacturer's protocol. RNU-48 was used to normalize the Ct values between the samples. In experiments involving miR analysis of exosomes, synthetic C. elegans (cel)-miR-39 was spiked during the total RNA isolation process and used as normalizer. All experiments were performed in triplicate. miR levels were normalized and the relative expression levels of specific miR were presented by $2^{-\Delta\Delta Ct}$.

MTT assay

CAL27 of HTB-43 cells were plated in 96-well plates. After 24 h, transfection with 25 nM of miR-34a-5p mimic or control mimic (Ambion) was performed with Lipofectamine RNAiMAX (Thermofisher). 3-(4,5-Dimethylthiazol-2-yl)-2,5-diphenyltetrazolium bromide assay was performed using the Vybrant® MTT Cell Proliferation Assay Kit, as described by the manufacturer. The absorbance of the samples was measured at 595 nm using a microtiter plate reader. Experiments were assayed in triplicate.

Apoptosis detection assay

Apoptosis levels were measured using an Annexin A5 apoptosis detection Kit (BioLegend) according to the manufacturer's protocol. HTB-43 and CAL27 cells were pretreated with miR-34a mimic using electroporation. Cells were collected after 48 h and the treated cells were washed twice with cold

BioLegend's Cell Staining Buffer and then resuspended in Annexin V Binding Buffer at a concentration of 0.25-1.0 × 10 cells/mL. After incubating for 15 min (25 °C), the cells were subjected to flow cytometry analysis to detect the apoptosis.

Antibodies and reagents

The following primary antibodies were used for this study: c-Met Monoclonal Antibody (3D4) (37–0100 ; Invitrogen); AGO2 Monoclonal Antibody (MA5-23515, Invitrogen); mouse IgG (sc-2025; Santa Cruz) anti-STAT3 Phospho (Tyr705) Antibody (13A3-1, Biolegend); anti-mouse CD45 Antibody (30-F11, Biolegend); anti-mouse CD206 (MMR) Antibody (C068C2; Biolegend); anti-mouse F4/80 Antibody (BM8; Biolegend); anti-mouse FOXP3 antibody (MF-14; Biolgened), anti-mouse CD25 (MF-14; Biolegend), anti-mouse CD4 (MF-14; Biolegend), anti-mouse lineage cocktail (145-2C11; RB6-8C5; RA3-6B2; Ter-119; M1/70; Biolegend) and anti-mouse CD274 (10F.9G2; Biolegend). hsa-miR-34a mimic and inhibors were obtained from Ambion (Thermofisher). pLL3.7 was a gift from Luk Parijs (Addgene plasmid # 11795). pLL3.7 hsa-miR-34a was a gift from Judy Lieberman (Addgene plasmid # 25791). Lipofectamin RNAiMAX (Thermofisher) was used for transfection experiments.

Cell lines

CAL27 was obtained from ATCC(CRL-2095™) and maintained in Dulbecco's minimal essential medium (DMEM). FADU was obtained from ATCC (HTB-43™) and maintained in ATCC-formulated Eagle's Minimum Essential Medium (EMEM). HCSS-4 was obtained from ATCC(CRL-1582™) and maintained in ATCC-formulated RPMI-1640 Medium. THP-1 was obtained from ATCC (TIB-202™) and maintained in ATCC-formulated RPMI. All cells were supplemented with 10% fetal bovine serum, 100 U/mL penicillin and 100 mg/mL streptomycin and incubated at 37 °C in 5% CO_2.

RNA immunoprecipitation (RIP)-PCR

Cells were cross-linked and lysed in IP buffer supplemented with phosphatase/protease inhibitors and RNase inhibitor. Cell lysates were sonicated and 100 ug of total protein was incubated with Ago2 antibody or mouse IgG (non-specific control), the lysates were incubated overnight with either 10ug/ml of ChIP-grade anti-Ago2 or mouse IgG in 4 °C for 90 min, followed by addition of Protein A/G PLUS-Agarose beads and incubation for 80 min. After washing, the eluted RNA samples were further purified with TRI reagent and subjected to TaqMan MicroRNA assay and real-time RT-PCR analysis to detect has-miR-34a-5p and MET, respectively. Data was normalized based on the total input.

Flow cytometry

A flow cytometry panel consisting of Lin-1, CD45, CD206, F4/80, and CD274 was used for quantification and characterization of tumor-associated macrophages. CD25, CD4, and FOXP3 were used for the identification of T-regs. Tumor cells were dissociated using our laboratory standard protocol [85]. For intracellular staining, cells were prepared using the Fix and Perm Kit (Invitrogen). Antibody-capture beads (CompBeads, BD Biosciences) were used as single-color compensation controls. Cytometer calibration was performed daily by the use of rainbow fluorescent particles (BD Biosciences), after acquiring

unstained and single-color control samples to calculate the compensation matrix. Data were analyzed using FCS Express software.

Statistical analysis

Student t-tests were performed to compare miR-34a expression level between classes in TCGA data, with $p < 0.05$ considered significant. To identify mRNA expression patterns that significantly correlate with miR-34 expression, a Pearson's correlation was performed, and p-values were corrected using FDR and Bonferroni methods. For experimental data, Parametric Student's t test or Mann-Whitney U test were performed for comparing two groups. Data are demonstrated as mean ± standard error of mean (SEM). P values less than 0.05 were considered as statistically significant.

Results

miR-34a is downregulated in different cancers, including breast cancer, lung cancer, bladder cancer, and pancreatic cancer (5, 42, 43). We analyzed the expression of miR-34a in TCGA tumor samples. As miR-34a is a transcriptional target of TP53, we compared miR-34 levels in cases with and without p53 mutation and found significantly lower miR-34a expression in p53 mutated cases compared to p53 WT cases ($P < 0.001$) (Fig. 1A). Similarly, in an SCC or HNSCC specific analysis, we found significantly lower expression of miR-34a in cases with p53 mutation ($P < 0.001$) (Fig. 1B and 1C). Interestingly, 1p chromosome deletion in non-mutated p53 cases was associated with a lower level of miR-34a in the pan-cancer analysis ($P < 0.0001$) (Fig. 1D). 1p chromosome deletion was associated with a lower level of miR-34a in SCCs ($P < 0.001$) (Fig. 1E), lung squamous cell carcinoma ($P < 0.05$) (Fig. 1F), and HNSCC cases (N.S.) (Fig. 1G). No statistically significant differences of miR-34a expression were detected between gain of chromosome 1p or wildtype (WT) chromosome 1p.

We next assessed the gene expression correlations with miR-34a expression in HNSCC patients in the TCGA dataset. For each mRNA, we calculated a Pearson correlation coefficient measuring its correlation with miR-34a expression, with Bonferroni-corrected p-values (**Supplemental Table 1A**). The correlation coefficients with a Bonferroni p-value below 0.01 were assessed for gene set enrichment in the hallmark and positional gene sets using the gene set enrichment analysis (GSEA) pre-ranked algorithm (Subramanian et al., 2005). The epithelial-mesenchymal transition (EMT) hallmark pathway was the top anti-correlation (Fig. 1H, **Supplementary Tables 1B and 1C, Supplemental Fig. 1**), including genes such as SNAI2, ZEB1, ZEB2, TWIST2, and TGFB1. This pathway is down-regulated when miR-34a expression is high, consistent with a role of miR-34a in inhibition of EMT.

The sequences of mature miR-34a-3p (passenger strand) and miR-34a-5p (guide stand) are conserved among species (44). Bioinformatic sequence analysis revealed that the MET 3' UTR has a binding motif for both miR-34a-3p and miR-34a-5p with high stability (mirSVR score of -0.9210 and PhastCons score of 0.7245 for miR-34a-5p and miRSVR score of -1.1609 and PHastCons score of 0.7019 for miR-34a-3p). (Fig. 2A, 2B). mirSVR score ≤ -0.1 and conserved sites indicated by PhastCOns score > 0.57 were reported as high predictor of miR-mRNA interaction (45). We analyzed levels of miR-34a-3p and miR-34a-5p in our

primary head and neck cancer patient tumor samples compared to adjacent tissue (n = 42). Levels of both miR-34a-5p and miR-34a-3p were decreased in tumor tissue compared to normal tissue ($P < 0.05$) (Figs. 2C and 2D). miR-34a levels in plasma isolated from HNSCC patients (n = 28) were also lower than in plasma from patients without HNSCC ($P < 0.05$) (n = 14; Figs. 2E and 2F). Moreover, levels of miR-34a-5p and miR-34a-3p were significantly lower in the circulating exosomes of patients with head and neck cancer compared to cancer-free patients ($P < 0.05$) (Figs. 2G and 2H).

Checking for absolute quantification of miR-34a-3p and miR-34a-5p in cancerous and healthy tissue, we found about a 50% reduction in miR-34a-5p and miR-34a-3p copy number in cancer tissue compared to the normal keratinocytes and normal tissue (**Supplemental Fig. 3**). However, miR-34a-3p copy number was overall much lower than miR-34a-5p, which could be attributed to the less stability of the passenger strand in miR biogenesis (46). As our bioinformatic prediction suggested direct targeting of MET by miR-34a-5p, we investigated MET expression in HNSCC samples. Using immunohistochemistry, we found that levels of MET expression were inversely associated with miR-34a-5p (Fig. 3A). We found a significant negative correlation between expression of MET and miR-34a in HNSCC cases of TCGA data (Bonferroni corrected $P < 0.0001$) (Fig. 3B). These correlations were likely not due to MET copy number variation; copy number variation for MET in HNSCC were so rare that only 4 out of 497 HNSCC samples in TCGA had high MET amplification. In addition, analysis of HNSCC samples with no MET copy number alteration still showed a significant negative correlation between miR-34a expression and MET expression ($P < 0.0001$) **(Supplemental Fig. 2)**. In immunohistochemistry of an oral squamous cell carcinoma, the whole width of the epithelial layer was positive for MET staining in contrast to partial staining in oral dysplastic tissue and negative staining in adjacent normal tissue (Fig. 3C). Interestingly, MET high expression was associated with a significantly lower survival rate in females compared to males in HNSCC, based on TCGA data ($P < 0.05$) (Fig. 3D). High expression of MET in HNSCC was associated with poor survival when stratifying by race, based on TCGA data ($P < 0.05$) (Fig. 3E).

We next studied the interaction of miR-34a-5p with MET in head and neck cancer cell lines. To investigate the direct interaction of miR-34a-5p with MET mRNA, we performed pulldown experiments with biotinylated miR-34a-5p or negative control probes and quantified levels of mRNA in the pulldown by qRT-PCR. We observed a dose-dependent enrichment of MET mRNA with miR-34a-5p probes suggesting a direct interaction (Fig. 4A). miRs exert their gene expression regulatory function through translational inhibition or transcript degradation via Argonaute 2 (AGO2)-catalyzed cleavage (47). Thus, we assessed the association of Ago2 with miR-34a-5p and MET to determine whether miR-34a was recruiting AGO2 to MET mRNA. Overexpression of miR-34a-5p by plasmid followed by anti-Ago2 CHIP and RIP-PCR on the whole cell lysate showed a complex of MET, miR-34a-5p with Ago2 in CAL27 cells. (Fig. 4B&4C).

Next, we assessed whether miR-34a-5p level correlated with MET mRNA expression in the HNSCC cell lines. The level of miR-34a-5p was down in all the head and neck cancer cell lines examined compared to oral keratinocytes (Fig. 4F), and the mRNA levels of MET were elevated in those cell lines (Fig. 4G). **As a more direct test to assess the effect of higher miR-34a on MET levels, we introduced** a miR-34a-5p mimic

in CAL27 cells, which resulted in a decrease of MET mRNA and protein levels (Fig. 4H&I). The results were similar in HTB-43 cell lines (data not shown).

miR-34a has been suggested to play a significant role in cancer cell proliferation, apoptosis, and migration (47). Thus, we further investigated the role of miR-34a in head and neck carcinogenesis using a miR-34a-5p mimic, a synthetic miR. Upon administration of the mimic in 2 different head and neck squamous cell lines (HTB-43, CAL27), measurement of annexin V and propidium iodide staining demonstrated an increase in the percentage of early apoptotic cells (Fig. 5A-5C). Introduction of the miR-34a-5p mimic led to dose-dependent inhibition of proliferation in the CAL27 cell line ($P < 0.05$) (Fig. 5D,5E) and HCSS-4 cell line **(Supplementary Fig. 4)**. In a xenograft model of head and neck cancer, administration of miR-34 mimic by IV injection significantly inhibited tumor growth ($P < 0.05$) (Fig. 5F).

To determine whether any of the effects of MET overexpression are dependent on miR-34a, we generated CAL27 cells with MET overexpression compared to control transduction (Fig. 6A). MET overexpression induced cell growth and proliferation that was attenuated by miR-34a-5p transient introduction (Fig. 6B). In addition, our rescue experiment demonstrated that the anti-apoptotic effect of MET overexpression can be reversed by miR-34a-5p overexpression (Fig. 6C).

As our bioinformatics analysis showed negative correlations of miR-34a with expression of epithelial-to-mesenchymal transcription factors such as SNAI2, ZEB1, ZEB2, and TWIST2, we assessed expression changes of epithelial and mesenchymal markers upon miR34a expression. As it has previously been shown that activated MET induces tumor invasion via phosphorylation of STAT3, we assessed levels of phospho-STAT3 (p-STAT3) and found decreased p-STAT3 after introduction of miR-34a-5p mimic in CAL27 cell lines (Fig. 6D). Interestingly, administration of miR-34a-5p led to a decreased expression of the mesenchymal marker vimentin and increased expression of epithelial marker CDH1 in head and neck cancer cell lines (CAL27 and SCC4) (Fig. 6E&6F), consistent with inhibition of EMT.

As the tumor microenvironment is composed of different cell types and miR-34a plays a role in tissue homeostasis, we evaluated the correlation between miR-34a expression and cellular subtypes in TCGA data. The cellular subtype estimates were generated by xCell (38). Among the top hits, higher expression of miR-34a was correlated with a significantly higher level of pro-B cells [p(FDR) = 4.42E-13], CD8 naïve T-cells [p(FDR) = 0.008] and Th1 cells [p(FDR) = 3.83E-7] in HNSCC tumors (**Supplementary Table 2A**, Fig. 7A, **Supplementary Figs. 5A and 5B)**. Interestingly, higher expression of miR-34a was associated with lower levels of T regulatory cells (Tregs) [p(FDR) = 1.9E-5], mast cells [p(FDR) = 1.73E-09] and monocytic cells [p(FDR) = 0.003] **(Supplementary Table 2B**, Fig. 7B-7D**).**

We next assessed the direct effect of miR-34a on immune cells in a FaDu xenograft mouse model of HNSCC. A single dose of the 15-mer LNA-antimiR-34a-5p inhibited expression of miR-34a in peripheral blood mononuclear cells (PBMCs) isolated from the bone marrow in 4 days. Administration of LNA-antimiR-34a-5p (subcutaneous) was associated with an increased presence of anti-inflammatory (M2-like) tumor associated macrophages (TAMs) ($CD45^+F4/80^+CD206^+$) in the tumor compared to the control

LNA inhibitor (Fig. 7E). Interestingly, the percentage of PDL1^{+}M2-like TAMs was significantly increased in the tumor tissue after LNA-antimiR-34a administration (Fig. 7F-7G). PDL1 expressing M2-TAMs are significantly associated with increased immune evasion and more aggressive lung cancers. In addition, PDL1 has been reported as one of the targets of miR34a (48–50). Interestingly, consistent with the TCGA data, administration of LNA-antimiR-34a in BALB/C mice resulted in an increased Treg expansion in the bone marrow **(Supplementary Fig. 6).** These data indicate a mechanistic role for miR-34a in promoting an immunosuppressive phenotype in the tumor microenvironment.

Discussion

MicroRNAs play an important role in the progression of HNSCC tumorigenesis and growth (28, 30, 51–53). It has been suggested that specific miRs could act as a molecular diagnostic tool for head and neck squamous cell carcinoma, (54, 55) and miR-based therapy could potentially be a rational approach for the therapeutic targeting of HNSCC (56). Identifying novel targets that would be efficient in HNSCC therapy is critical. In the present study, for the first time, we investigated the role of the miR-34a-MET axis in the pathogenesis of HNSCC. Our analysis of TCGA data demonstrated that downregulation of miR-34a is associated with P53 mutation and chromosome arm 1p deletion in HNSCC and lung squamous cell carcinoma. Additionally, higher levels of miR-34a were correlated with lower levels of key transcription factors of EMT. We found significantly decreased levels of miR-34a in tumor tissue and circulation of patients with HNSCC. We found that miR-34a acts as a tumor suppressor, directly represses the proto-oncogene MET, and modulates cell proliferation. Lastly, our work demonstrates a role of miR-34a in maintaining tumor immunity, as inhibition of miR-34a resulted in a decreased in percentage of anti-inflammatory (M2-like) TAMs and PDL1^{+}TAMs, which are reported to have pro-tumorigenic activity (57, 58).

miR-34a is down-regulated in many cancers (47, 59–61), and there are several hypotheses that explain this down-regulation (48, 62–64). By leveraging the TCGA dataset, we demonstrated two possible mechanisms of miR-34a down-regulation in cancer. p53 mutation correlates with decreased expression of miR-34a, consistent with previous work establishing miR-34a as a transcriptional target of p53. In addition, miR-34a is located on chromosome 1p, a chromosome arm that is frequently deleted in cancer (13). We also demonstrated that chromosome 1p deletion correlates with decreased miR-34a expression. This is not surprising, as DNA copy number generally correlates with gene expression, but also suggests chromosome arm-level deletion could serve as a biomarker for response to miR-34a-based therapeutic approaches. We are actively pursuing aneuploidy as a biomarker for drug response, including for miR-34a and other miRs. Interestingly, the effect of copy number on miR-34a expression is masked by p53 mutation; if p53 is mutated, there is no correlation between chromosome 1p copy number and miR-34a expression. These data are consistent with *trans* transcriptional regulation serving a more important role than *cis* DNA levels.

Our mechanistic experiments showed that miR-34a directly interacts with the proto-oncogene MET and attenuates the MET signaling axis by posttranscriptional gene regulation in cancer cells. Activating point

mutations of MET and MET amplification have been reported in several cancer types, including gastric cancer (65), breast cancer (66), hepatocellular carcinoma (67, 68) and non-small cell lung cancer (69, 70). MET plays an important role in the occurrence, development, invasion and metastasis of malignant tumors (69, 71–73). While MET is a validated drug target in lung cancer, the best biomarker strategy for enrichment of a susceptible patient population still remained undefined (69), and its role in HNSCC was not well known. We found high expression of MET throughout the entire epithelium in oral cancer in contrast to a partial staining in oral dysplastic lesions and no expression in normal tissue. The mechanistic role of MET in the transformation of pre-cancerous lesions to cancerous lesions should be further investigated in future studies. Additionally, we found a correlation between MET high expression levels and unfavorable survival outcomes, particularly in females with HNSCC.

Direct interaction of mir-34a with PDL1 has been reported previously (48). The role of the PDL1- PD1 axis in facilitating tumor escape from immune control has led to an active therapeutic target in multiple cancer types (74, 75). However, the fact that PDL1 is expressed not only in cancer cells but also in immune cells with the highest abundance in TAMs has only been recently reported (49, 76, 77). TAMs are one of the major cell populations in the tumor microenvironment (78) and express the vast majority of PDL1 in tumors. The level of PDL1 expression in TAMS could determine efficacy of PDL1 pathway blockade (49, 57). TAMs that express PDL1 can suppress T cells in the tumor microenvironment and contribute to tumor immune evasion (79, 80).

Our analysis of TCGA data showed that increased expression of miR-34a is correlated with decreased Tregs and monocytic cells, consistent with our experimental model of the HNSCC tumor in mouse. Interestingly, our experimental data demonstrated that miR-34a inhibition perturbs anti-tumor immunity by increasing the percentage of M2-TAMs and $PDL1^{+}$TAMs in mice. This study presents strong evidence that miR-34a overexpression may have a potential therapeutic benefit in HNSCC via MET inhibition and restoration of anti-tumor immunity. In particular, miR-34a overexpression might be useful as an adjuvant therapy or monotherapy in HNSCC.

The pleiotropic nature of miRs and their involvement in all cancer hallmarks makes them particularly attractive drug targets for cancer treatment. A challenge of miR-based therapy is the delivery of miRs in the right dose to the target tissue. Different drug delivery vehicles have been proposed for miR delivery, including liposomes and exosomes. Liposomes are immunogenic, subject to rapid clearance by the immune system after administration (81). In contrast, exosomes, naturally occurring nanovesicles, are not immunogenic and can be used effectively for miR-based therapy (82). Another strategy is chemical modification of miR-mimics or inhibitors to induce higher stability and cell penetration. In the accessible solid tumors, intra-tumoral injections of miR-based therapies into the pathogenic site could improve efficacy and minimize side effects (83). In the present study we showed that restoration of miR-34a could inhibit tumor growth and progression and restore anti-tumor immune function in HNSCC. Our data provide evidence that miR-34a might be a suitable target for HNSCC treatment.

Conclusions

miR-34a acts as a tumor suppressor and physically interacts with and functionally targets the proto-oncogene MET. miR-34a expression is inversely correlated with MET in tumor tissue. miR-34a might be useful as an adjuvant therapy or monotherapy in HNSCC.

List Of Abbreviations

HNSCC Head and Neck Squamous Cell Carcinoma

miR : microRNA

TCGA: The Cancer Genomic Atlas

TAMs: Tumor Associated Macrophages

EMT: Epithelial-to-Mesenchymal Transition

PDL1: Programmed Death Ligand 1

3'UTR: 3' Untranslated region

LNA: Locked Nucleic Acid

PBMC: Peripheral Blood Mononuclear Cell

FDR: False Discovery Rate

AGO2: Argonaute 2

GSEA: Gene Set Enrichment Analysis

SEM: Standard error of mean

qPCR: Quantitative Real-Time Polymerase Chain Reaction

RIP-PCR: RNA Immunoprecipitation- Polymerase Chain Reaction

EMEM: Eagle's Minimum Essential Medium

DMEM: Dulbecco'S Minimal Essential Medium

Declarations

Ethics approval and consent to participate

The research proceeded according to the ethics approval of Columbia University Irving Medical Center. All animal use and experiments were performed in strict accordance with the procedures approved by the

Animal Care and Use Committee (ACUC).

Consent for publication

All participants provided informed written consent.

Competing interests

The authors declare that they have no competing interests.

Funding

This research was funded by grants from the Columbia University Irving Medical Center, the Columbia University College of Dental Medicine, and the Irving Institute for Clinical and Translational Research (UL1 TR001873) and NIH/NIDCR (DE029546-01) to FMH. These studies used the Herbert Irving Comprehensive Cancer Center Flow Cytometry Shared Resource, Biomarker Shared Resources, and Molecular Pathology Shared Resources funded in part through a Center Grant (P30 CA013696) from the NIH.

Authors' contributions

X.W, S.B, and FMH performed the experiments, Y-LC, AY, M.M, GKS, A.T, and FMH helped with sample collection, data analysis, and data interpretation. A.T performed bioinformatic analysis on TCGA data. X.W, A.T, and F.M.H wrote the manuscript. A.T, and F.M.H revised and finalized the manuscript.

Acknowledgments

Not applicable.

References

1. Dhawan A, Scott JG, Harris AL, Buffa FM. Pan-cancer characterisation of microRNA across cancer hallmarks reveals microRNA-mediated downregulation of tumour suppressors. Nat Commun. 2018;9:5228.
2. Slabáková E, Culig Z, Remšík J, Souček K. Correction Alternative mechanisms of miR-34a regulation in cancer. Cell Death Dis. 2018;9:783.
3. Welponer H, Tsibulak I, Wieser V, et al. The miR-34 family and its clinical significance in ovarian cancer. J Cancer. 2020;11:1446–56.
4. Lopez CM, Yu PY, Zhang X, Yilmaz AS, London CA, Fenger JM. MiR-34a regulates the invasive capacity of canine osteosarcoma cell lines. PLoS One. 2018;13:e0190086.
5. Hasakova K, Reis R, Vician M, Zeman M, Herichova I. Expression of miR-34a-5p is up-regulated in human colorectal cancer and correlates with survival and clock gene PER2 expression. PLoS One. 2019;14:e0224396.

6. Juracek J, Stanik M, Vesela P, et al. Tumor expression of miR-34a-3p is an independent predictor of recurrence in non-muscle-invasive bladder cancer and promising additional factor to improve predictive value of EORTC nomogram.Urol Oncol,2019;37:184.e1-184.e7.
7. Kim JS, Kim EJ, Lee S, et al. MiR-34a and miR-34b/c have distinct effects on the suppression of lung adenocarcinomas. Exp Mol Med. 2019;51:1–10.
8. Li Z, Chen H. miR-34a inhibits proliferation, migration and invasion of paediatric neuroblastoma cells via targeting HNF4α. Artif Cells Nanomed Biotechnol. 2019;47:3072–8.
9. Weng YS, Tseng HY, Chen YA, et al. MCT-1/miR-34a/IL-6/IL-6R signaling axis promotes EMT progression, cancer stemness and M2 macrophage polarization in triple-negative breast cancer. Mol Cancer. 2019;18:42.
10. Zheng SZ, Sun P, Wang JP, Liu Y, Gong W, Liu J. MiR-34a overexpression enhances the inhibitory effect of doxorubicin on HepG2 cells. World J Gastroenterol. 2019;25:2752–62.
11. Zhu M, Wu J, Ma X, et al. Butyl benzyl phthalate promotes prostate cancer cell proliferation through miR-34a downregulation. Toxicol In Vitro. 2019;54:82–8.
12. Zuo Y, Zheng W, Liu J, Tang Q, Wang SS, Yang XS MiR-34a-5p/PD-L1 axis regulates cisplatin chemoresistance of ovarian cancer cells.Neoplasma,2020;67:93–101.
13. Taylor AM, Shih J, Ha G, et al. Genomic and Functional Approaches to Understanding Cancer Aneuploidy. Cancer Cell. 2018;33:676–89.e3.
14. Busch M, Klein S, Große-Kreul J, et al. p53, miR-34a and EMP1-Newly Identified Targets of TFF3 Signaling in Y79 Retinoblastoma Cells.Int J Mol Sci,2019;20.
15. Cerna K, Oppelt J, Chochola V, et al. MicroRNA miR-34a downregulates FOXP1 during DNA damage response to limit BCR signalling in chronic lymphocytic leukaemia. B cellsLeukemia. 2019;33:403–14.
16. Upadhyay P, Sarker S, Ghosh A, et al. Transferrin-decorated thymoquinone-loaded PEG-PLGA nanoparticles exhibit anticarcinogenic effect in non-small cell lung carcinoma via the modulation of miR-34a and miR-16. Biomater Sci. 2019;7:4325–44.
17. Slabáková E, Culig Z, Remšík J, Souček K. Alternative mechanisms of miR-34a regulation in cancer. Cell Death Dis. 2017;8:e3100.
18. Jauhari A, Singh T, Singh P, Parmar D, Yadav S. Regulation of miR-34 Family in Neuronal Development. Mol Neurobiol. 2018;55:936–45.
19. Siemens H, Neumann J, Jackstadt R, et al. Detection of miR-34a promoter methylation in combination with elevated expression of c-Met and β-catenin predicts distant metastasis of colon cancer. Clin Cancer Res. 2013;19:710–20.
20. Zhou Y, Ding BZ, Lin YP, Wang HB. MiR-34a, as a suppressor, enhance the susceptibility of gastric cancer cell to luteolin by directly targeting HK1.Gene2018;644:56–65.
21. Sullivan KD, Galbraith MD, Andrysik Z, Espinosa JM. Mechanisms of transcriptional regulation by p53. Cell Death Differ. 2018;25:133–43.

22. Okada N, Lin CP, Ribeiro MC, et al. A positive feedback between p53 and miR-34 miRNAs mediates tumor suppression. Genes Dev. 2014;28:438–50.
23. Jiang D, Li M, Yu Y, Shi H, Chen R. microRNA-34a aggravates coxsackievirus B3-induced apoptosis of cardiomyocytes through the SIRT1-p53 pathway. J Med Virol. 2019;91:1643–51.
24. Dai X, Li M, Geng F. Omega-3 Polyunsaturated Fatty Acids Eicosapentaenoic Acid and Docosahexaenoic Acid Enhance Dexamethasone Sensitivity in Multiple Myeloma Cells by the p53/miR-34a/Bcl-2. AxisBiochemistry (Mosc). 2017;82:826–33.
25. Zhu JN, Fu YH, Hu ZQ, et al. Activation of miR-34a-5p/Sirt1/p66shc pathway contributes to doxorubicin-induced cardiotoxicity. Sci Rep. 2017;7:11879.
26. Hart M, Walch-Rückheim B, Krammes L, et al. miR-34a as hub of T cell regulation networks. J Immunother Cancer. 2019;7:187.
27. Xiao X, Gu Y, Wang G, Chen S, c-Myc. RMRP, and miR-34a-5p form a positive-feedback loop to regulate cell proliferation and apoptosis in multiple myeloma. Int J Biol Macromol. 2019;122:526–37.
28. Momen-Heravi F, Bala S. Extracellular vesicles in oral squamous carcinoma carry oncogenic miRNA profile and reprogram monocytes via. NF-κB pathwayOncotarget. 2018;9:34838–54.
29. Metheetrairut C, Chotigavanich C, Amornpichetkul K, Keskool P, Ongard S, Metheetrairut C. Expression levels of miR-34-family microRNAs are associated with TP53 mutation status in head and neck squamous cell carcinoma. Eur Arch Otorhinolaryngol. 2019;276:521–33.
30. Yoon AJ, Wang S, Kutler DI, et al. MicroRNA-based risk scoring system to identify early-stage oral squamous cell carcinoma patients at high-risk for cancer-specific mortality.Head Neck,2020.
31. Wang Y, Chen J, Chen X, et al. MiR-34a suppresses HNSCC growth through modulating cell cycle. arrest senescenceNeoplasma. 2017;64:543–53.
32. Hajalirezay Yazdi S, Paryan M, Mohammadi-Yeganeh S. An integrated approach of bioinformatic prediction and in vitro analysis identified that miR-34a targets MET and AXL in triple-negative breast cancer. Cell Mol Biol Lett. 2018;23:51.
33. Liu H, Deng H, Zhao Y, Li C, Liang Y. LncRNA XIST/miR-34a axis modulates the cell proliferation and tumor growth of thyroid cancer through MET-PI3K-AKT signaling.J Exp. Clin Cancer Res. 2018;37:279.
34. Sun Z, Zhang T, Chen B, Long Non-Coding RNA. Metastasis-Associated Lung Adenocarcinoma Transcript 1 (MALAT1) Promotes Proliferation and Metastasis of Osteosarcoma Cells by Targeting c-Met and SOX4 via miR-34a/c-5p and miR-449a/b. Med Sci Monit. 2019;25:1410–22.
35. Zhao M, Wang Y, Liu Y, et al. C7 peptide inhibits hepatocellular carcinoma metastasis by targeting the HGF/c-Met signaling pathway. Cancer Biol Ther. 2019;20:1430–42.
36. www.Clinicaltrilas.gov NCT02862145.
37. Li F, Li X, Qiao L, Liu W, Xu C, Wang X. MALAT1 regulates miR-34a expression in melanoma cells. Cell Death Dis. 2019;10:389.

38. Aran D, Hu Z, Butte AJ. xCell: digitally portraying the tissue cellular heterogeneity landscapeGenome Biol. 2017;18:220.
39. Chandrashekar DS, Bashel B, Balasubramanya S, et al. UALCAN: A Portal for Facilitating Tumor Subgroup Gene Expression and. Survival AnalysesNeoplasia. 2017;19:649–58.
40. Subramanian A, Kuehn H, Gould J, Tamayo P, Mesirov JP. GSEA-P: a desktop application for Gene. Set Enrichment AnalysisBioinformatics. 2007;23:3251–3.
41. Bernardo BC, Gao XM, Winbanks CE, et al. Therapeutic inhibition of the miR-34 family attenuates pathological cardiac remodeling and improves heart function. Proc Natl Acad Sci U S A. 2012;109:17615–20.
42. Sun X, Huang T, Liu Z, Sun M, Luo S. LncRNA SNHG7 contributes to tumorigenesis and progression in breast cancer by interacting with miR-34a through EMT initiation and the Notch-1 pathway. Eur J Pharmacol. 2019;856:172407.
43. Xin X, Lin F, Wang Q, Yin L, Mahato RI. ROS-Responsive Polymeric Micelles for Triggered Simultaneous Delivery of PLK1 Inhibitor/miR-34a and Effective Synergistic Therapy in Pancreatic Cancer. ACS Appl Mater Interfaces. 2019;11:14647–59.
44. Li XJ, Ren ZJ, Tang JH. MicroRNA-34a: a potential therapeutic target in human cancer. Cell Death Dis. 2014;5:e1327.
45. Betel D, Wilson M, Gabow A, Marks DS, Sander C. The microRNAorg resource: targets expressionNucleic Acids Res. 2008;36:D149–53.
46. Guo L, Lu Z. The fate of miRNA* strand through evolutionary analysis: implication for degradation as merely carrier strand or potential regulatory molecule. PLoS One. 2010;5:e11387.
47. Wang B, Li D, Kovalchuk I, et al. miR-34a directly targets tRNAiMet precursors and affects cellular proliferation, cell cycle, and apoptosis. Proc Natl Acad Sci U S A. 2018;115:7392–7.
48. Cortez MA, Ivan C, Valdecanas D, et al. PDL1 Regulation by p53 via miR-34.J Natl Cancer Inst,2016;108.
49. Lin H, Wei S, Hurt EM, et al. Host expression of PD-L1 determines efficacy of PD-L1 pathway blockade-mediated tumor regression. J Clin Invest. 2018;128:805–15.
50. Sumitomo R, Hirai T, Fujita M, Murakami H, Otake Y, Huang CL. PD-L1 expression on tumor-infiltrating immune cells is highly associated with M2 TAM and aggressive malignant potential in patients with resected non-small cell lung cancer. Lung Cancer. 2019;136:136–44.
51. Ganci F, Sacconi A, Manciocco V, et al. Altered peritumoral microRNA expression predicts head and neck cancer patients with a high risk of recurrence. Mod Pathol. 2017;30:1387–401.
52. Chanatip M, Chanticha C, Kanchana A, Phawin K, Sunun O, Choakchai M. Expression levels of miR-34-family microRNAs are associated with TP53 mutation status in head and neck squamous cell carcinoma.Eur Arch Otorhinolaryngol,2018.
53. Momen-Heravi F, Bala S. Emerging role of non-coding RNA in oral cancer. Cell Signal. 2018;42:134–43.

54. Cristaldi M, Mauceri R, Di Fede O, Giuliana G, Campisi G, Panzarella V. Salivary Biomarkers for Oral Squamous Cell Carcinoma Diagnosis and Follow-Up. Current Status PerspectivesFront Physiol. 2019;10:1476.
55. Rock LD, Minatel BC, Marshall EA, et al. Expanding the Transcriptome of Head and Neck Squamous Cell Carcinoma Through Novel MicroRNA Discovery. Front Oncol. 2019;9:1305.
56. Fadhil RS, Wei MQ, Nikolarakos D, Good D, Nair RG. Salivary microRNA miR-let-7a-5p and miR-3928 could be used as potential diagnostic bio-markers for head and neck squamous cell carcinoma. PLoS One. 2020;15:e0221779.
57. Noguchi T, Ward JP, Gubin MM, et al. Temporally Distinct PD-L1 Expression by Tumor and Host Cells Contributes to Immune Escape. Cancer Immunol Res. 2017;5:106–17.
58. Bordon Y. Pro-tumour programming at the macrophage membrane. Nat Rev Immunol. 2019;19:270–1.
59. Bao Y, Lu Y, Feng W, et al. COUP–TFII promotes epithelial–mesenchymal transition by inhibiting miR–34a expression in colorectal cancer. Int J Oncol. 2019;54:1337–44.
60. Kapadia CH, Ioele SA, Day ES. Layer-by-layer assembled PLGA nanoparticles carrying miR-34a cargo inhibit the proliferation and cell cycle progression of triple-negative breast cancer cells. J Biomed Mater Res A. 2020;108:601–13.
61. Li Y, Hu H, Wang Y, et al. CUL4B contributes to cancer stemness by repressing tumor suppressor miR34a in colorectal cancer.Oncogenesis,2020;9:20.
62. Öner MG, Rokavec M, Kaller M, et al. Combined Inactivation of TP53 and MIR34A Promotes Colorectal Cancer Development and Progression in Mice Via Increasing Levels of IL6R and PAI1.Gastroenterology2018;155:1868–1882.
63. Li Q, Wang C, Cai L, et al. miR–34a derived from mesenchymal stem cells stimulates senescence in glioma cells by inducing. DNA damageMol Med Rep. 2019;19:1849–57.
64. Yang G, Fu Y, Lu X, Wang M, Dong H, Li Q. miR–34a regulates the chemosensitivity of retinoblastoma cells via modulation of MAGE–A/p53 signaling. Int J Oncol. 2019;54:177–87.
65. Wei B, Huang QY, Huang SR, Mai W, Zhong XG. MicroRNA–34a attenuates the proliferation, invasion and metastasis of gastric cancer cells via downregulation of. METMol Med Rep. 2015;12:5255–61.
66. Parsons BM, Meier DR, Richmond CS, et al. Acquisition of Cabozantinib-Sensitive MET D1228N Mutation During Progression on Crizotinib in MET-Amplified Triple-Negative Breast Cancer.Clin Breast Cancer,2020.
67. Li N, Fu H, Tie Y, et al. miR-34a inhibits migration and invasion by down-regulation of c-Met expression in human hepatocellular carcinoma cells. Cancer Lett. 2009;275:44–53.
68. Li P, Zhang J, Li F, Yu Y, Chen Y. Low–intensity ultrasound enhances the chemosensitivity of hepatocellular carcinoma cells to cisplatin via altering the miR–34a/c–Met axis. Int J Mol Med. 2019;44:135–44.

69. Schuler M, Berardi R, Lim WT, et al. Molecular correlates of response to capmatinib in advanced non-small-cell lung cancer: clinical and biomarker results from a Phase I trial.Ann Oncol,2020.
70. Shimokawa M, Nosaki K, Seto T, et al. Phase II, open-label, multicenter trial of crizotinib in Japanese patients with advanced non-small cell lung cancer harboring a MET gene alteration. Co-MET studyTrials. 2020;21:298.
71. Gherardi E, Birchmeier W, Birchmeier C, Woude V. G. Targeting MET in cancer: rationale and progress. Nat Rev Cancer. 2012;12:89–103.
72. Li Q, Hutchins AP, Chen Y, et al. A sequential EMT-MET mechanism drives the differentiation of human embryonic stem cells towards hepatocytes. Nat Commun. 2017;8:15166.
73. Li H, Li CW, Li X, et al. MET Inhibitors Promote Liver Tumor Evasion of the Immune Response by Stabilizing PDL1.Gastroenterology2019;156:1849–1861.e13.
74. Mahoney KM, Rennert PD, Freeman GJ. Combination cancer immunotherapy and new immunomodulatory targets. Nat Rev Drug Discov. 2015;14:561–84.
75. Daassi D, Mahoney KM, Freeman GJ. The importance of exosomal PDL1 in tumour immune evasion. Nat Rev Immunol. 2020;20:209–15.
76. Tseng YH, Ho HL, Lai CR, et al. PD-L1 Expression of Tumor Cells, Macrophages, and Immune Cells in Non-Small Cell Lung Cancer Patients with Malignant Pleural Effusion. J Thorac Oncol. 2018;13:447–53.
77. Liu Y, Zugazagoitia J, Ahmed FS, et al. Immune Cell PD-L1 Colocalizes with Macrophages and Is Associated with Outcome in PD-1 Pathway Blockade Therapy. Clin Cancer Res. 2020;26:970–7.
78. Rose M, Duhamel M, Aboulouard S, et al. The Role of a Proprotein Convertase Inhibitor in Reactivation of Tumor-Associated Macrophages and Inhibition of. Glioma GrowthMol Ther Oncolytics. 2020;17:31–46.
79. Latchman YE, Liang SC, Wu Y, et al. PD-L1-deficient mice show that PD-L1 on T cells, antigen-presenting cells, and host tissues negatively regulates T cells. Proc Natl Acad Sci U S A. 2004;101:10691–6.
80. Ding ZC, Lu X, Yu M, et al. Immunosuppressive myeloid cells induced by chemotherapy attenuate antitumor CD4 + T-cell responses through the PD-1-PD-L1 axis. Cancer Res. 2014;74:3441–53.
81. Semple SC, Harasym TO, Clow KA, Ansell SM, Klimuk SK, Hope MJ. Immunogenicity and rapid blood clearance of liposomes containing polyethylene glycol-lipid conjugates and nucleic Acid. J Pharmacol Exp Ther. 2005;312:1020–6.
82. Momen-Heravi F, Getting SJ, Moschos SA. Extracellular vesicles and their nucleic acids for biomarker discovery. Pharmacol Ther. 2018;192:170–87.
83. Chen Y, Gao DY, Huang L. In vivo delivery of miRNAs for cancer therapy: challenges and strategies. Adv Drug Deliv Rev. 2015;81:128–41.

Supplementary Files Note

SI tables 1 and 2 are missing from this manuscript version

Figures

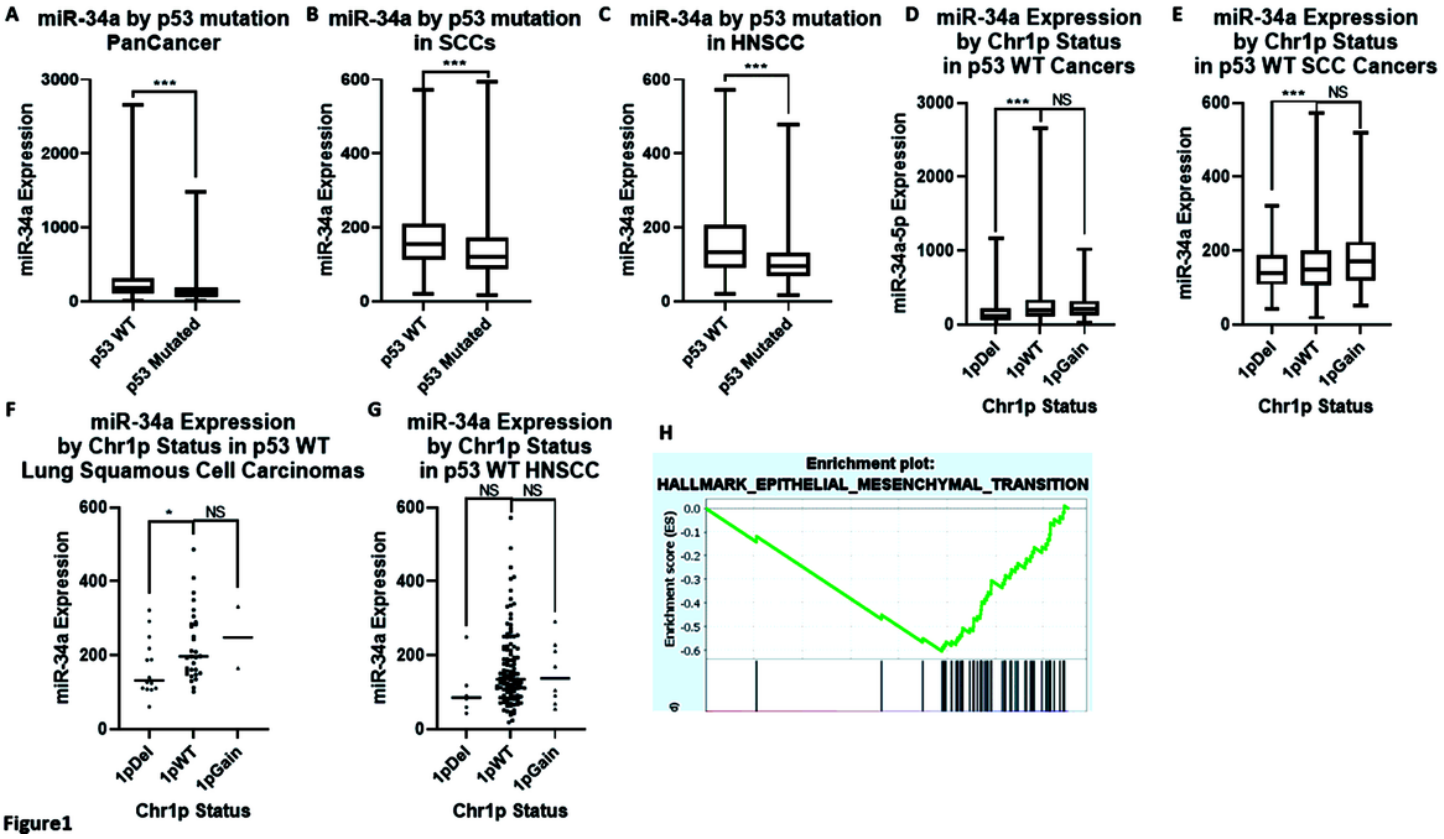

Figure 1

p53 mutation and chr1p deletion correlates with decreased miR-34a expression. A through C: miR-34a expression versus p53 mutation status in patient tumors across 33 cancer types (n=9151) (A), squamous cell carcinomas (n=1293) (B), or HNSCCs(n=490) (C). D through G: miR-34a expression versus chr1p copy number level in p53 WT tumors, across cancer (n=7792) (D), across squamous cancers (n=380) (E), in lung squamous cell carcinomas (n=380) (F), or HNSCCs (n=132) (G). (H): Genes whose expression significantly correlated with miR-34a expression were analyzed by gene set enrichment analysis (GSEA) in HNSCC samples (n = 497). Plot shows the top enriched hallmark pathway, Epithelial-Mesenchymal Transition (EMT). Y-axis is the GSEA enrichment score. X-axis is list of genes ranked by differential expression correlation with miR-34a, with black bars representing genes in the EMT gene set. * indicates $p<0.05$; *** indicates $p<0.001$.

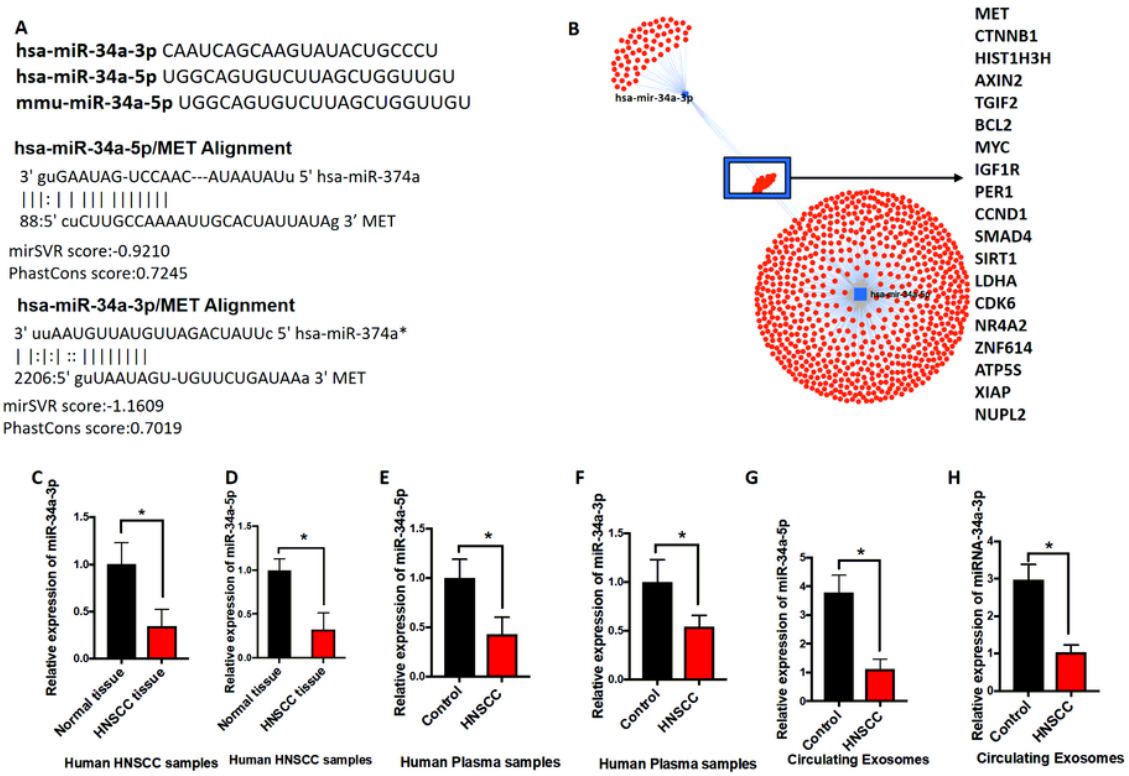

Figure 2

Figure 2

miR-34 is downregulated in head and neck cancer and targets proto-oncogene MET. (A) Sequence of the mature miR-34a-5p and miR-34a-5p in human and mouse. Bioinformatic analysis suggested direct interaction of both the miR-34a guide strand (hsa-miR-34a-5p) and passenger strand (hsa-miR-34a-3p) with the 3'UTR of MET mRNA. C through H: (Expression of miR-34a-3p and miR-34a-3p were quantified by the TaqMan miR Assay in HNSCC samples and matched controls (n=42) (C and D), HNSCC and healthy plasma (E and F) and exosomes (n=28) (G and H). 2-□□CT method was used for relative expression. Data was normalized to RNU48 or cel39. Data is presented as mean□SD. * indicates p<0.05.

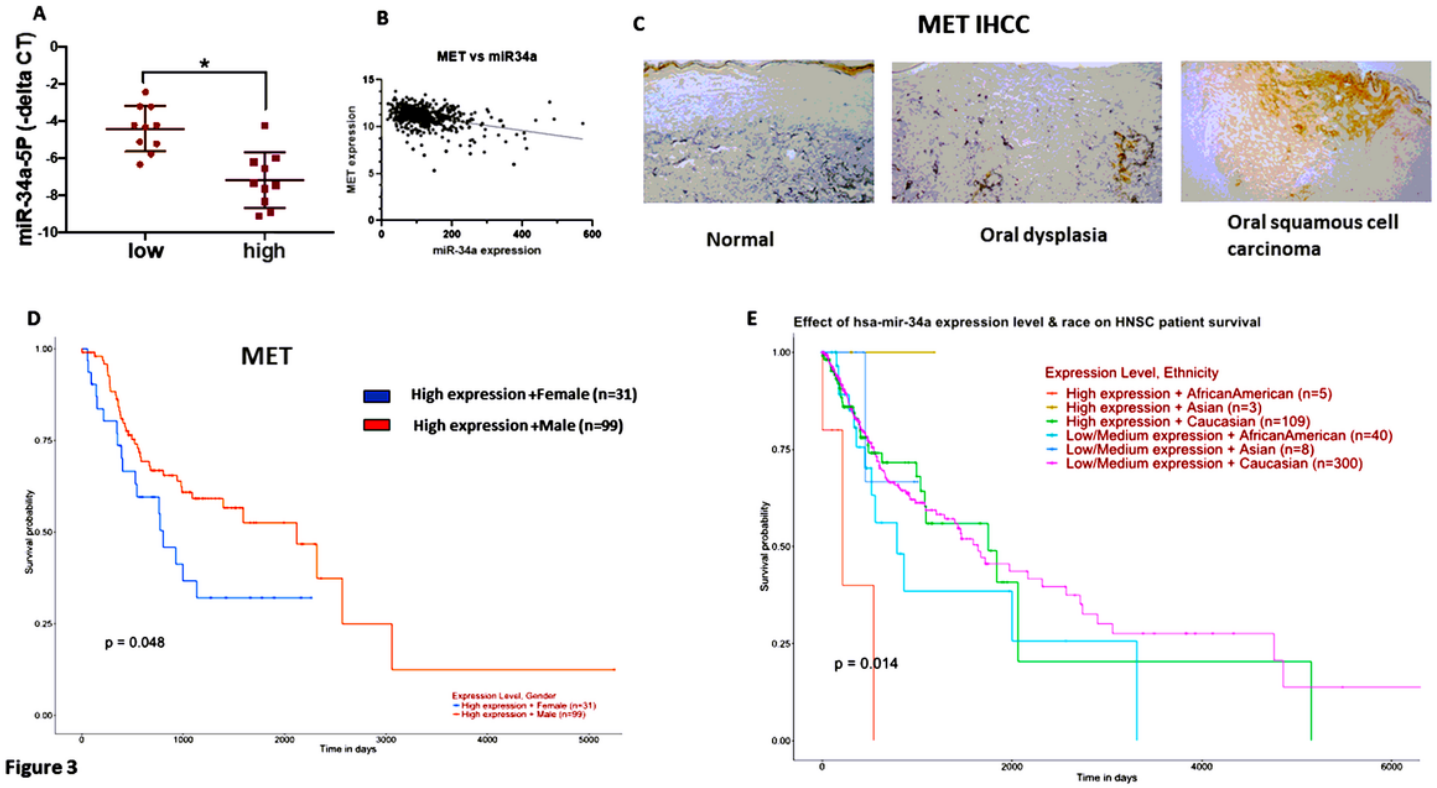

Figure 3

Levels of miR-34a negatively correlate with MET and MET expression correlates with patient survival. (A) miR-34a expression versus MET expression in HNSCC (n=20) (B) correlation of MET and miR-34a expression in over 497 HNSCC cancers in the TCGA dataset. (C) Immunohistochemistry of MET expression in normal tissue, dysplastic tissue and HNSCC tissue. (D) and (E) Survival of HNSCC patients based on MET expression stratified based on gender (n=120) and race (n=502). * indicates $p<0.05$.

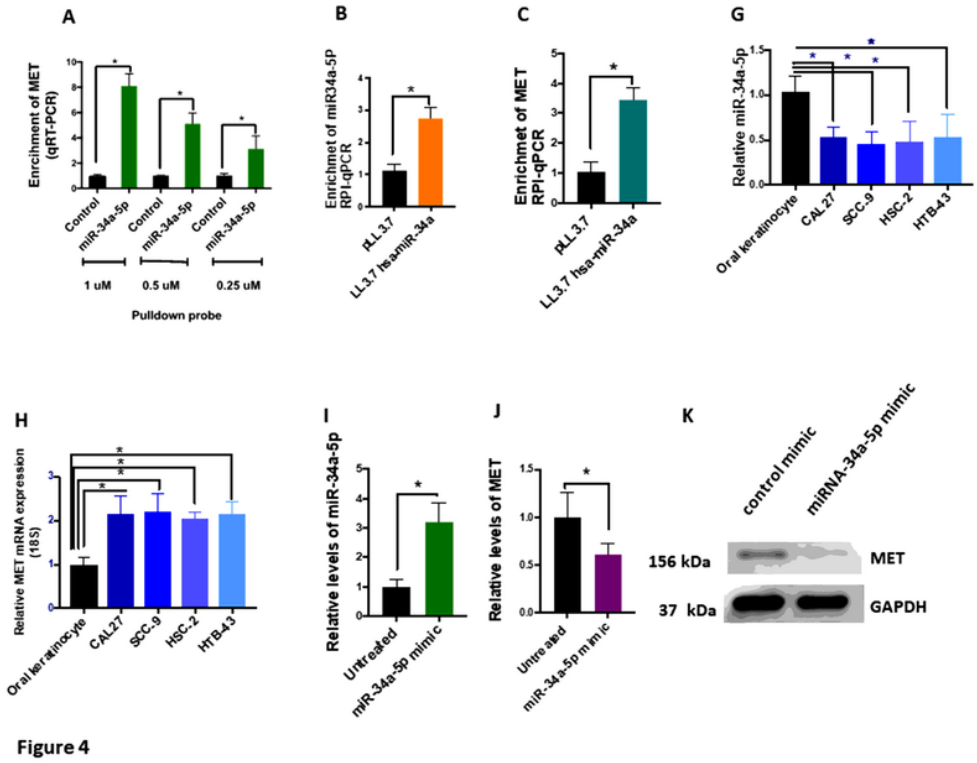

Figure 4

Figure 4

miR-34a directly interacts with MET mRNA and downregulates MET. (A) RNA was isolated from cells, biotin-based pull-down probe for miR-34a-5p or negative control probe at different concentrations to assess interaction of miR-34a-5p with MET in CAL27 cells was used. The enrichment of MET was quantified by qPCR. (B and C) The miR-34a-5p overexpressing CAL27 cells were subjected to an anti-Ago2 CHIP assay. Levels of MET and miR-34a-5p were quantified by qPCR. (G and H) MET expression and miR-34a-5p expression in HNSCC cell lines. (I) Quantification of miR-34a-5p overexpression by miR mimic. (J) Over-expression of miR-34a-5p mimic lead to decrease in MET expression levels after 24h. (K) Western blot measuring MET protein with and without expression of has-miR-34a-5p mimic. All experiments were performed in CAL27 cells. All experiments were performed in triplicate. Data is presented as mean□SD.* indicates $p<0.05$.

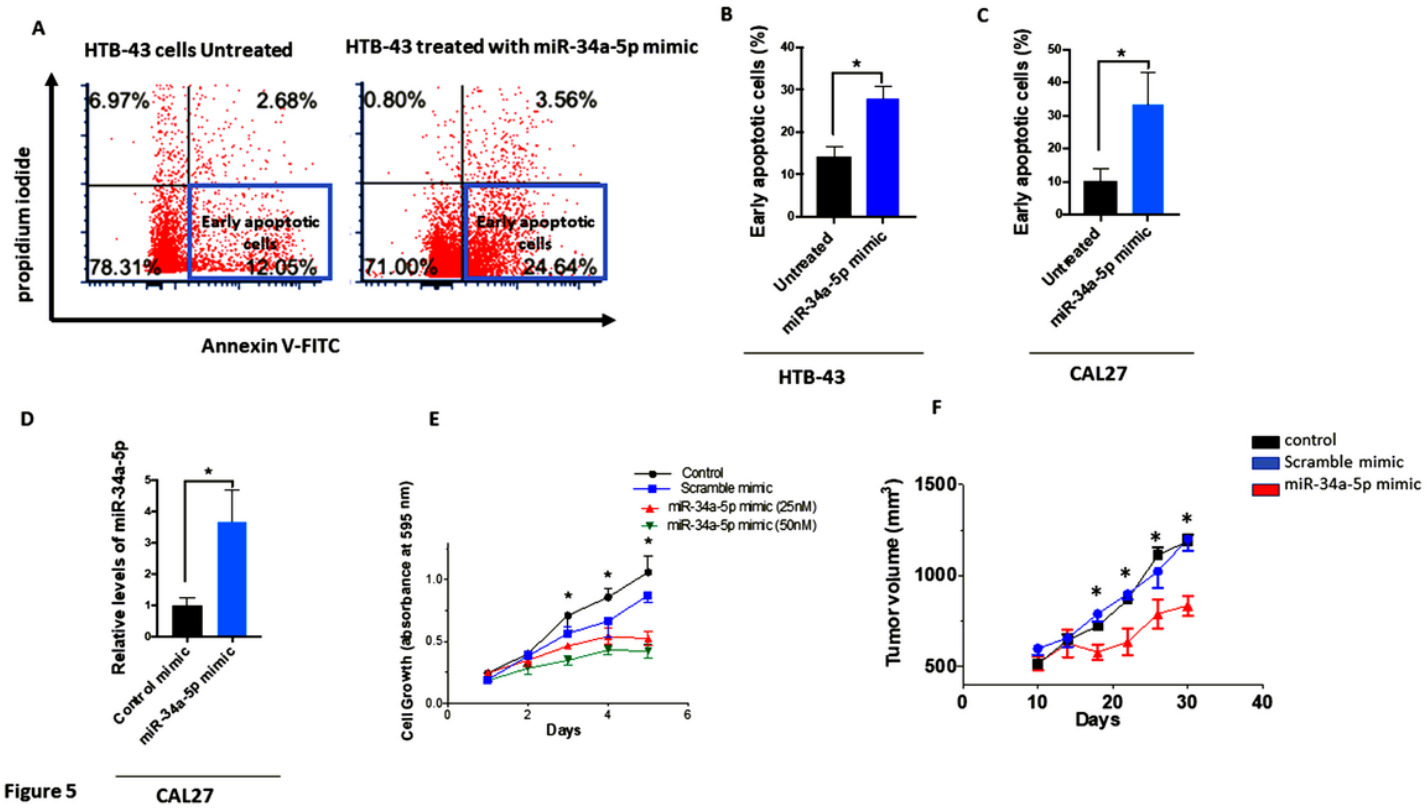

Figure 5

miR-34a over-expression induces early apoptosis, prevents tumor proliferation, and inhibits tumor growth in vivo. (A) Representative flow cytometry plot of annexin V (FITC) versus propidium iodide in control mimic treated cells or miR-34a-5p treated HTB-42 cells (25nM, 48h). Early apoptotic cells were defined as propidium iodide low and Annexin-V high. (B, C) Percentage of early apoptotic cells were determined by early apoptosis detection assay in 2 different head and neck squamous cell lines (HTB-43 and CAL27 cells). (D) Level of miR-34a-5p expression was determined by qPCR 12h post electroporation of miR-34a mimic or control mimic (25nM). (E) miR-34a mimic (25nM or 50nM) was administered to cells at day 0, and proliferation was measured using MTT reagent to assess the effect of miR-34a on proliferation of CAL27 cells. (F) Effect of miR-34a-5p mimic in tumor growth in FADU xenograft model of head and neck cancer (n=18), days versus tumor volume. miRNA mimic (1 µ mole) or control mimic (1 µ mole) were loaded into THP derived exosomes and injected to the mice every 48h. Data is presented as mean□SD.* indicates $p<0.05$.

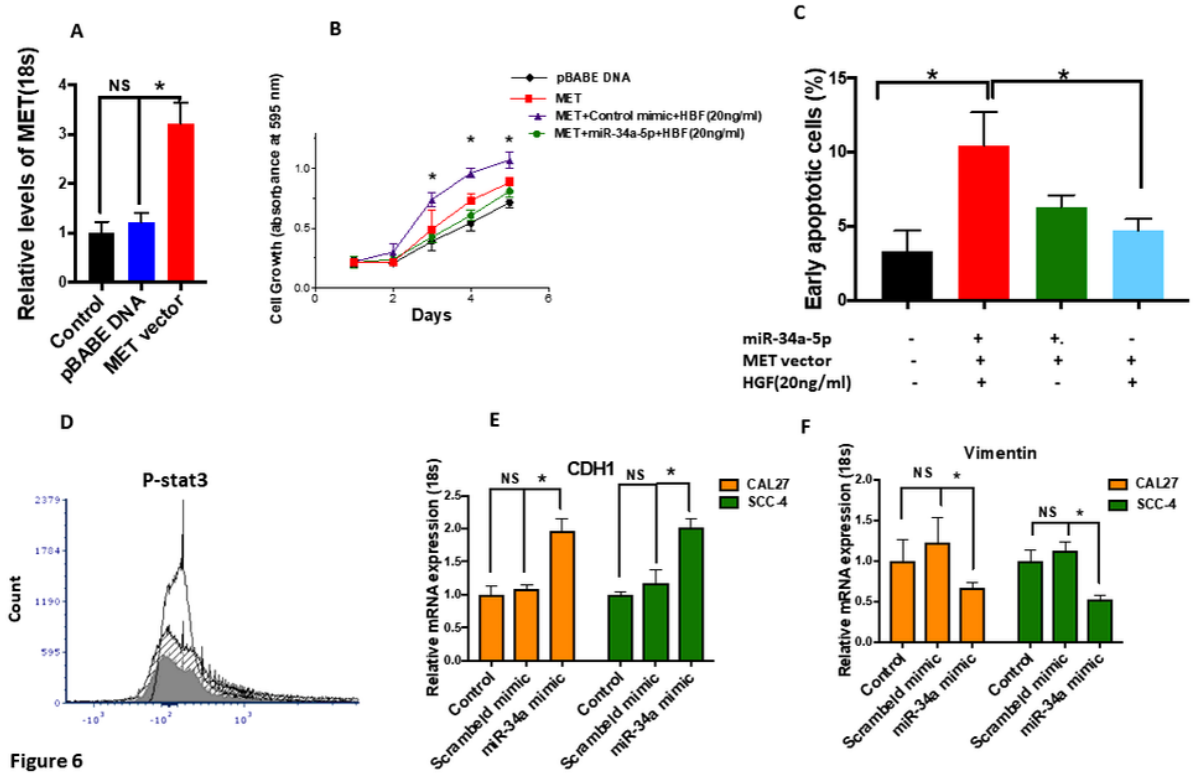

Figure 6

Figure 6

The anti-tumorigenic effect of miR-34a is dependent on MET, and miR-34a inhibits epithelial mesenchymal transition. (A) MET vector or control vector (pBABE) were introduced to CAL27 cells and levels of MET expression were quantified by qPCR. (B) miR-34a (25nM) mimic was administrated to the MET overexpressing CAL27 cells and cell proliferation was measured after 24h using MTT assay. (C) Percentage of early apoptotic cells were determined by Annexin V and PI in MET overexpressing CAL27 cells with and without introduction of miR-34a-5p mimic. MET signaling was stimulated with HGF. (D) Effect of miR-34a on STAT3 phosphorylation (shaded line: control; open line: HGF (20ng); gray line: HGF (20ng)+miR34a mimic). (E, F) Relative mRNA expression of epithelial marker (CDH1) and mesenchymal marker (Vimentin) when a scrambled mimic or miR-34a mimic is overexpressed. Data is presented as mean□SD. * indicates $p<0.05$.

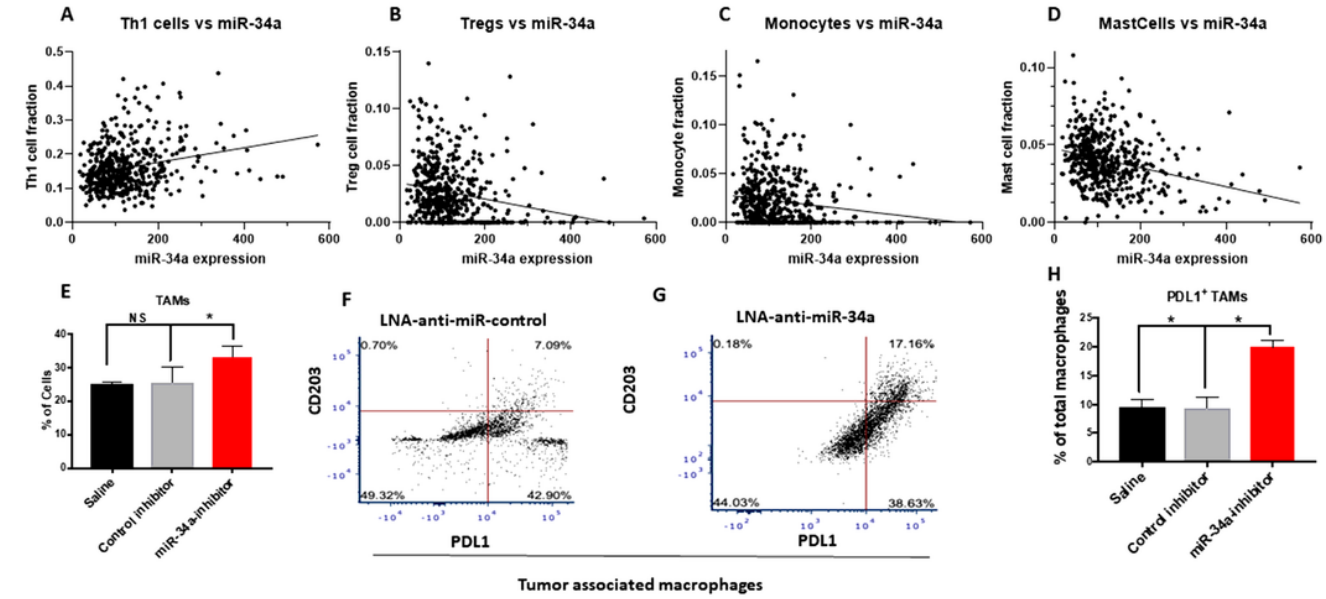

Figure 7

Figure 7

Lower miR-34 levels are correlated with an increase in immunosuppressive tumor microenvironment and tumor associated macrophages. (A-D) Levels of immune cell sample infiltration were compared to miR-34a expression levels in TCGA HNSCC (n=497). X-axis is mi-34a expression, y-axis is fraction of cell type present in the sequenced tumor sample (E) LNA-miR-34a inhibitor or control inhibitor were injected to the xenograft mice model of head and neck cancer. Tumor was dissociated using a tumor dissociation kit and single cell suspension was prepared. Percentage of M2- like TAMs (F4/80+CD206+) were identified by flow cytometry. Gating was performed on CD45+cells and live cells (n=14). (F-G) Representative graph of PDL1 expressing M2-TAMs in control miR inhibitor or LNA-miR-34a inhibitor injected mice (n=16). X-axis is PD-L1, y-axis is CD203. (H) Total percentage of PDL1+TAMs were quantified in CD45+cells by flow-cytometry. Data is presented as mean SD.*indicates $p<0.05$.

Supplementary Files

This is a list of supplementary files associated with this preprint. Click to download.

- supplfigure1.tif
- supplfigure2.tif
- supplfigure3.tif
- supplfigure4.tif

- supplfigure5.tif
- supplfiguure6.tif